Machine Learning for Deep Brain Stimulation Efficacy using Dense Array EEG

Morgan Stuart, Chathurika S. Wickramasinghe, Daniel L. Marino,
Deepak Kumbhare*, Kathryn Holloway*, Milos Manic
Department of Computer Science & Department of Neurosurgery*
Virginia Commonwealth University
Richmond, Virginia
stuartms@vcu.edu, brahmanacsw@vcu.edu, marinodl@vcu.edu,
kumbharedw@vcu.edu, kathryn.holloway@vcuhealth.org, misko@ieee.org

***Abstract*—Deep brain stimulation (DBS) is well recognized as an effective treatment for symptoms of movement disorders such as Parkinson's disease (PD), Essential Tremor, and dystonia. The selection of the appropriate contact on the DBS lead for optimal clinical efficacy can be challenging, particularly when considering directional leads. Electroencephalograms (EEG) and electrocorticography has been utilized to better understand the pathophysiology of PD but a methodology to provide an objective biomarker of effective stimulation has yet to be developed.**

Using machine learning techniques for feature extraction and classification, we contrast high resolution EEG captured during DBS against its resting state counterpart with the DBS off. We demonstrate, using 16 patients under DBS treatment for movement disorders, EEG's informative capacity to detect both effective DBS and the region undergoing stimulation.

I. Introduction

Applied DBS has had success in treatment of movement disorders such as Parkinson's disease (PD) [1–6], Essential Tremor (ET) [7–10], and dystonia [11][12]. The electrical stimulation of motor nuclei such as globus pallidus interna (GPI), subthalamic nucleus (STN), and ventral intermedius nucleus (VIM) of the thalamus generates an active volume around the electrode site modulating the neuronal tissue in that region. With therapeutic high frequency (125-185 Hz) stimulation, the relay of pathological signals through the subcircuitries in the basal ganglia thalamocortical network is altered, ultimately alleviating the underlying motor symptoms. Previous work has shown a pathological coupling between phase and amplitude of EEG within the motor cortex [13][14]. Both DBS and dopaminergic medicines result in a return to a more normal EEG pattern [13–16].

DBS treatment begins with surgery to implant leads in the brain region appropriate for the desired effect. The DBS leads have contacts over the distal 9mm of the implanted lead (Medtronic Inc.). These leads are connected to implanted generators which can be programmed at any time after surgery, altering contact location, amplitude, pulse width, and stimulation frequencies [17–19]. After recovery from surgery, selection of the most effective parameters for symptom controls is required.

In these mapping sessions, the response to varied stimulation configurations is empirically evaluated for efficacy by monitoring patient response in real time. Side effects are simply brain responses other than the ones desired for efficacy. For instance, the contact in the ventral posterolateral (VPL) nucleus of the thalamus will elicit tingling in the contralateral hand or face, the contact in the VIM will stop the patient's tremor, and a contact within the internal capsule will elicit facial contraction [20]. All of these effects are routinely elicited during the mapping process.

While mapping and configuring the leads can often be straightforward, it is ultimately a visual-qualitative interpretation performed by an expert. The process can be hampered when application of the stimulation has delayed effects, such as DBS of the GPI region [21]. Occasionally, the patient will have side effects that cannot be easily categorized and can be related to anxiety or heightened awareness of internal stimuli [18] [19]. A comprehensive review of the complexities encountered during programming is given in [22]. It follows that an objective criteria for DBS efficacy could help reduce the configuration search space and improve the process.

In order to objectively identify the optimal response to DBS, we are exploring the utility of Quantitative EEG (QEEG) feature extraction and analysis. EEG-based methods have advantages over other techniques, such as Positron Emission Tomography (PET), as the data can be acquired and analyzed repeatedly during a programming session as different parameters are selected and evaluated. Although PET scans have the ability to assess metabolic changes associated with DBS, this exposes the patient to radiation, and it cannot be used in an iterative process. Similarly the oxygen metabolic changes identified with fMRI are radically constrained by the MRI environment and slower time course. Finally, the incorporation of EEG is relatively low cost.

In this work, machine learning based feature extraction and classification methods are applied to high resolution EEG data captured from 16 patients with DBS implants. Patients are fitted with a dense array EEG cap with 256 channels. EEG is recorded as the DBS mapping procedure cycles through stimulus configurations. For each patient, EEG data is also captured without DBS being applied. The resulting dataset is annotated for the location of the lead within the basal ganglia/thalamus and the clinical efficacy of the DBS parameters.

With this dataset, we explore the informative capacity of

EEG to assist in DBS treatment. Specific problems include whether DBS is being optimally applied and what aspects of brain activity are affected during DBS. We consider these challenges through two separate classification tasks: (1) Detecting active stimulation and (2) classifying the region of the brain undergoing stimulation. We compare resulting performance and features selected, split across three stimulation regions and 16 patients. Our results demonstrate the clear potential for reliable classification within these tasks, with both detection of DBS across patients and DBS region discrimination consistently achieving precision over 0.6 while still maintaining useful recall.

II. Related Work

Early efforts to decode the EEG response of the brain to DBS concentrated on the peak amplitude and latencies of the evoked response (EP) in the area of the motor cortex. Work in [10][23][24] provides insight into similarities and differences between the various locations of the implanted stimulator. In contrast to the extensive study of EPs to STN stimulation, much less has been explored with GPI EPs, with existing work focusing on dystonia patients [25][26].

Source localization algorithms have been useful in identifying the affected EP in both the anatomic and time domains. Laxton et al mapped the brain areas that are affected by electrical stimulation of the fornix in AD patients [27][28], demonstrating activation of the ipsilateral hippocampal formation and the medial temporal lobe. This data was consistent with the PET data in the same patients. The technique has also been used in mapping the response to Brodman area Cg 25 for the treatment of depression [29].

Beta oscillations have long been recognized as the idling rhythm of the motor cortex. The discovery of the beta band in the STN region of Parkinsonian patients brought renewed focus to this unique oscillation and its potential role in PD pathophysiology. De Hemptine et al [16] has demonstrated that STN DBS reduces this excessive phase amplitude coupling seen in PD. Although the original experiments were conducted intra-operatively using electrocorticography, a similar finding has been demonstrated noninvasively with EEG while analyzing the effect of medications on the excessive phase amplitude coupling (PAC)[13][14]. This study demonstrated increased PAC off medications as compared to on medication as well as controls. This work suggests that the EEG signature of effective DBS stimulation may be disease specific rather than nucleus specific, with effective stimulation resulting in alteration of the abnormal oscillatory characteristics of the patient's disease state.

In general, this work continues the trend of applied QEEG techniques that have been popular for brain computer interfacing, including motor imagery [30–32], spike detection [33][34], and transcranial stimulation [35]. Finally, while this work focuses on EEG data, other inputs for assessing effectiveness, such as video monitoring [36][37], may prove valuable in future work.

TABLE I
Summary of Patients

ID	Stim. Region	DBS Type	On/Off Length	Partition
1	GPI	Bilateral	02:16 / 01:48	Train
2	STN+VIM	Bilateral	02:00 / 01:38	Train
3	VIM	Left	02:04 / 01:52	Holdout
4	GPI	Bilateral	04:46 / 04:22	Holdout
5	GPI	Bilateral	02:50 / 02:30	Train
6	GPI	Bilateral	01:56 / 02:08	Train
7	STN	Bilateral	02:00 / 01:58	Holdout
8	VIM	Bilateral	02:22 / 01:42	Train
9	VIM	Bilateral	03:54 / 03:46	Train
10	GPI	Bilateral	02:12 / 02:22	Holdout
11	VIM	Bilateral	03:44 / 04:44	Holdout
12	GPI	Bilateral	03:54 / 02:20	Train
13	VIM	Bilateral	01:32 / 09:14	Train
14	VIM	Left	04:02 / 04:14	Holdout
15	GPI	Bilateral	01:26 / 02:54	Train
16	GPI	Bilateral	05:04 / 01:26	Holdout

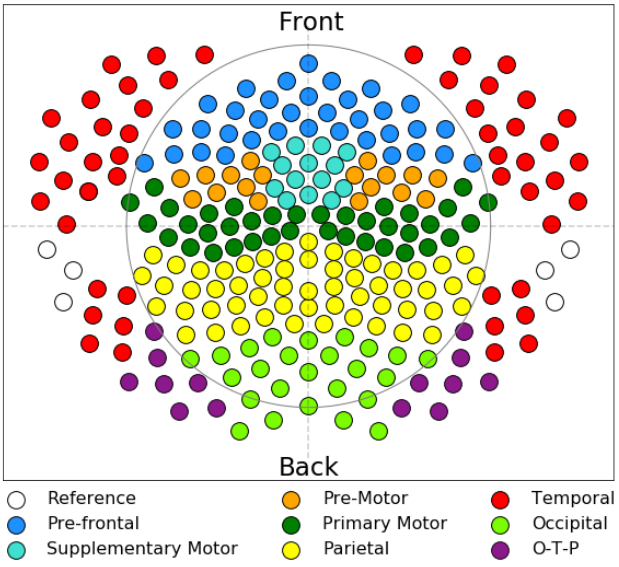

Fig. 1. (Best viewed in color) 2-Dimensional layout of 256 EEG sensors and their corresponding brain regions.

III. Data Collection

A total of 16 patients participated in the data collection procedure, each with stimulus in either the GPI, VIM, or STN regions of the brain. There are 8 patients with GPI DBS (6 PD, 1 dystonia, 1 Tourettes), 6 patients with VIM DBS (2 PD, 4 ET), 1 patient with STN DBS (PD), and 1 PD patient with VIM on the right and STN on the left.

EEG data acquisition is performed with an Electrical Geodesisc Inc Dense Array system containing 256 sensors, sampled at 1KHz using the EGI GTEN 100 Amplifier via the EGI NetStation 5 software. For optimal contact each patient's head circumference is measured for the most appropriate size net of sensors. A 2D projection of electrode placements and brain regions are illustrated in Figure 1.

EEG data is first recorded while the technician monitors for artifacts and adjusts sensors in real time to address issues.

Next, DBS is turned off and EEG is captured for 2-5 minutes or as long as tolerable to the patient. With the baseline collected, the electrode mapping begins in a standard fashion while EEG data is collected. Once an optimal response is achieved, another 2-5 minutes of data is recorded.

After initial data collection, the recording session is segmented into several smaller datasets. These include segments of optimal DBS response resulting from successful mapping, poor DBS response encountered during mapping, and periods when DBS is switched off. In this work, data segments captured when DBS is off are referred to as *DBS-OFF* and data captured during optimal DBS are referred to as *DBS-ON*.

IV. Preprocessing & Modeling Pipeline

The data undergoes several processing stages before being passed to a supervised classifier. These steps can be broadly categorized as part of either the preprocessing pipeline or the model pipeline, as illustrated in Figure 2. Section IV-A details the unsupervised preprocessing and Section IV-B describes target-oriented feature selection, extraction, and modeling.

Before processing, patient data are split into a train partition and a holdout partition. The partitioning is stratified across the stimulation region to ensure variations arising from the region are well-represented in both sets of samples. See Table I for a summary of each patient's stimulation region, type, experiment length (MM:SS), and partition. The train set is used to tune the overall pipeline, while the holdout set is reserved for the evaluation of the best performing processes developed on the train set.

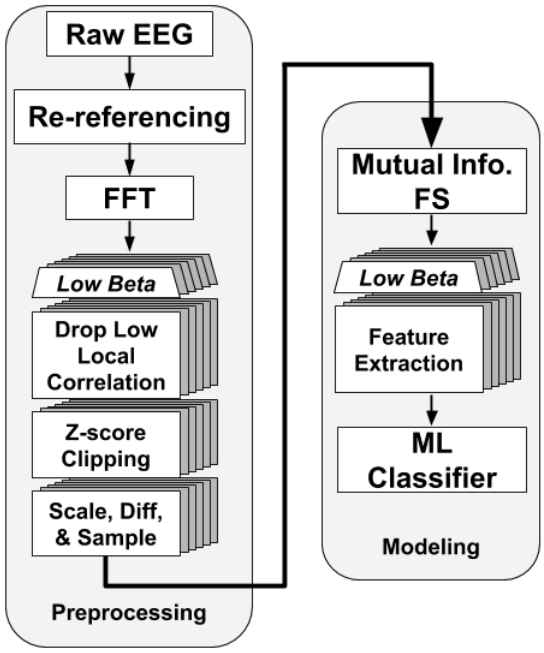

Fig. 2. Summary of model processing pipeline: Each sample of raw EEG is independently re-referenced before bands are extracted. Each band is separately treated for anomalies by dropping sensors with low local correlation and clipping sample values based on their modified Z-score. Each band is then rescaled by dividing by the max before being converted to deltas to remove level shifts. To balance the training set, 140 samples are drawn from each experiment with replacement. Bands are then recombined into a flattened set of samples before the top 25% of features are selected based on their mutual information with the target. Bands are then separated for band-wise feature extraction, before being recombined for input into an ML classifier.

A. Preprocessing Pipeline

The raw EEG voltages are first re-referenced to the average voltage of the sensors nearest the mastoids, since these sensors tend to receive reduced signal from the brain. Specifically, for each sample of 256 real-valued potentials, the sensors nearest the back of the ear are averaged and the resulting mean is subtracted from all sensors, including the reference sensors. The channels used as references are identified in Figure 1.

Next, the fast Fourier transform (FFT) is applied to the re-referenced EEG magnitudes. The FFT is applied in 1 second sliding rectangular windows with a step size of 1 second. From each channel, we extract the average response from 8 bands characterized by a center frequency f_0 and a bandwidth of 2Hz, yielding the region $[f_0 - 1, f_0 + 1)$. Center frequencies begin at 15Hz and continue in steps of 2Hz, ending with the inclusion of $f_0 = 29$Hz. The FFT's windowing procedure and the band extraction reduces the number of samples and increases the number of features, making conservative anomaly detection and feature selection critical for reliable results.

Next, anomaly detection must be applied in order to remove artifacts arising from physiological differences or irregularities in electrode connectivity. The first step of automatic anomaly detection is applied to the bands retrieved from the FFT process. We examine spatially local correlation to identify sensors that behave poorly over time. This is approached by calculating the Pearson correlation coefficient for the r_n nearest sensors to each sensor. Distance is measured on the 2D plane shown in Figure 1 using Euclidean distance. Any sensor with a median neighbor correlation less than a specified positive outlier threshold, r_T, is considered anomalous. This rule is derived from the spatial locality of sensors, which generally results in a strong correlation over time between neighboring sensors. We select $r_n = 7$ and then calculate $r_T = 0.72$ as the 90th percentile of median neighbor correlation for all sensors across all experiments in the training set.

Sensors failing the local correlation threshold in the train set are dropped from the remainder of the processing for that band in all datasets. We choose this treatment, rather than imputation, to leverage the redundancy of the 256 channel EEG and to avoid introducing unwanted bias from imputation. However, since only the training partition is used to identify poorly correlated sensors, new correlation anomalies in the holdout must be imputed. Therefore, sensors identified as anomalous through local correlation in the holdout are replaced with the median value from their r_n neighboring sensors at each sample. This is performed before dropping sensors in the holdout that were identified in the train set.

After addressing sensors that behave poorly over time using local correlation, we examine each sensor value with respect to the distribution of values captured by a sensor in an experiment. We use the modified Z-score, defined in Equation

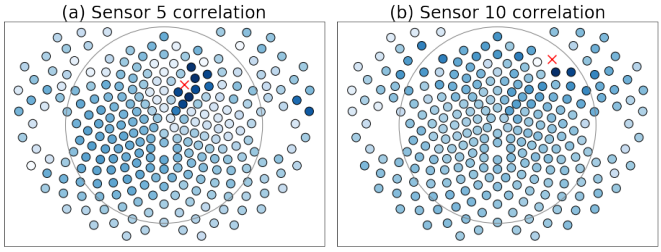

Fig. 3. Example of correlation-based outlier detection using patient 5's DBS-OFF beta band. (a) Sensor 5 is highly correlated to most of its neighbors, while (b) sensor 10 is irregularly not correlated with its neighboring sensors.

1, to identify anomalous sensor values. The modified Z-score uses the median instead of the mean in its calculation, and is therefore well-suited for identifying outliers [38].

$$Z_{s_i} = \frac{x_{s_i} - median(x_s)}{1.4826 \times \mathrm{MAD_s}} \tag{1}$$

$$\mathrm{MAD_s} = median(|x_s - median(x_s)|) \tag{2}$$

Where x_s is all data for sensor s and x_{s_i} is the ith value for sensor s. We select $Z_{s_i} > 5$ as our threshold for outliers, such that each value outside this threshold is clipped to the range $[-Z_s = 5, Z_s = 5]$. Given equations 1 and 2, a unique threshold value, X_T, exists for each sensor across each experiment and is calculated using Equation 3:

$$X_T = 1.4826 \times 5 \times MAD_s + median(x_s) \tag{3}$$

Any value in a sensor with $|Z_s| > 5$ is replaced with the sensor's X_T. While this artificial ceiling will still carry some portion of its original information, it no longer has as large an influence on down-stream processing.

After clipping, each experiments' band-level datasets are scaled to the interval [0, 1] by dividing by each channel's respective maximums. A delta transform is then applied, taking the sample-to-sample difference through time. This centers the values around zero and helps remove any level shifts that may leak experiment information, without involving additional parameters. Finally, to balance the dataset and ensure fair representation, 140 samples are drawn (with replacement) from each band-level dataset for every experiment. This sampling procedure is only performed on the training set.

B. Modeling Pipeline

Following the preprocessing described in Section IV-A, the bands are recombined for univariate feature selection using mutual information (MI). For every feature, MI between the feature and the target is computed. The features are ranked by their MI score and the top 25% of features are kept. These features are then separated back into their respective bands before being passed to a model.

Each model is the combination of feature extractions at the band level concatenated and passed to a supervised classifier. We use the SciKit-Learn machine learning library [39] for feature extraction, modeling, and searching the hyperparameter space. Four feature extraction techniques are compared, including three unsupervised methods: principle component analysis (PCA), independent component analysis (ICA), and agglomerative feature clustering (FC) with mean pooling. Common Spatial Patterns (CSP) [40], a supervised technique popular in QEEG, is also included. Extracted features are passed to one of five supervised classification models. We compare logistic regression with L2 regularization (LR), classification from K-Neighbors' labels (KN), random and gradient boosted ensembles of trees (RF and GB), and Radial Basis Function (RBF) support vectors machine (SVM).

The four feature extraction methods and five model types result in 20 distinct extraction+classifier models to be examined and tuned. Due to the size of the search space, a randomized grid search is used to explore potential hyperparameters using K-Fold cross-validation on the training patients. Models are ranked and selected by their precision score. The folds are grouped at the patient level such that no patient's samples are included in both the holdout fold and the training folds. The K-fold strategy varies between the modeling task, so further detail is given in Section V. Feature extraction methodologies are not mixed in a single model, meaning only one of PCA, ICA, CSP, or FC is applied in a given model, but each band's extraction procedure has independent hyperparameters.

V. Modeling Results

Towards guided DBS for improved efficacy, we examine ML methodologies on two binary classification problems: detecting DBS and discriminating between regions of DBS across patients. Both problems are approached using the preprocessing and modeling pipelines described in Sections IV-A and IV-B, respectively. Once the best hyperparameters for each of the 20 extraction+classifier models are selected, we then select the best extraction method for each classifier based on cross-validation performance. These 5 resulting extraction+classifier models are then examined on the holdout partition to evaluate generalization performance.

A. Detecting DBS Across Patients

We first examine the ability to detect active DBS in a patient, regardless of DBS type. To accomplish this, the training cohort and their DBS-ON and DBS-OFF segments are combined into a single set of training samples. Samples taken from DBS-ON belong to the positive class, while DBS-OFF samples are assigned to the negative class. The resulting holdout dataset has a 0.51 target rate across 2,584 samples. The features selected, through anomaly treatment and then feature selection, are depicted in Figure 5. A 9-Fold, leave-one-patient-out cross-validation scheme is used in this experiment in order to encourage cross-patient generalization.

The best cross-validation results of the hyperparameter search are given in Table II. The holdout results for the top performing classifier+extration pairs are given in Table III, alongside the total number of features extracted across bands. We find that PCA-SVM and PCA-RF are most successful

TABLE II
STIMULATION DETECTION BEST CV PRECISION SCORES

	CSP	ICA	FC	PCA
GB	**0.83**	0.81	0.79	0.82
KN	0.70	0.68	0.68	0.69
LR	0.52	0.52	0.53	0.52
RF	0.82	**0.82**	**0.80**	0.82
SVM	0.75	0.57	0.83	**0.83**

TABLE III
STIMULATION DETECTION MODEL PERFORMANCE ON HOLDOUT PATIENTS

	N Extracted	**Accuracy**	**F1**	**Precision**	**Recall**
PCA - SVM	34	0.56	0.40	**0.73**	0.28
PCA - RF	36	**0.62**	**0.59**	0.70	0.51
FC - LR	32	0.49	0.51	0.52	0.51
CSP - KN	28	0.54	0.55	0.58	**0.52**
CSP - GB	48	0.53	0.45	0.61	0.36

regarding precision on the holdout set, but the SVM classifier only recalls less than a third of the positive samples, leaving PCA-RF with the highest F1 score. The CSP-KN model, a high bias estimator coupled with supervised extraction, achieves the best recall while still maintaining a competitive F1 score. We take the best performing model on the cross-validation set and produce a learning curve, shown in Figure 4, which appears to asymptote, suggesting the need for more informative features.

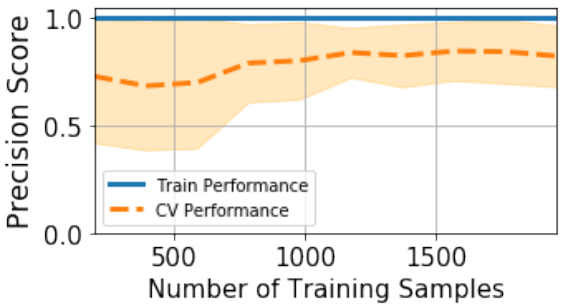

Fig. 4. Learning curve with 9-fold grouped cross-validation for DBS detection using CSP-GB model. A subtle upward trend in the validation data that levels off suggests the need for more meaningful features and better regularization.

B. Classifying DBS-ON Stimulation Region

Next, the ability for ML classifiers to separate active DBS on region is examined. For this experiment, only DBS-ON samples are utilized. Furthermore, while three separate stimulation regions are present in our dataset, STN is poorly represented with only two patients receiving this type of treatment, with one of these patients receiving both VIM and STN stimulation. For this reason, we combine VIM and STN treaments into a single class and contrast these samples against GPI treatments. Thus, we examine a binary classification task with GPI treatments assigned to the positive class and VIM+STN assigned to the negative class. The resulting holdout dataset has a 0.53 target rate in its 1,379 samples. The

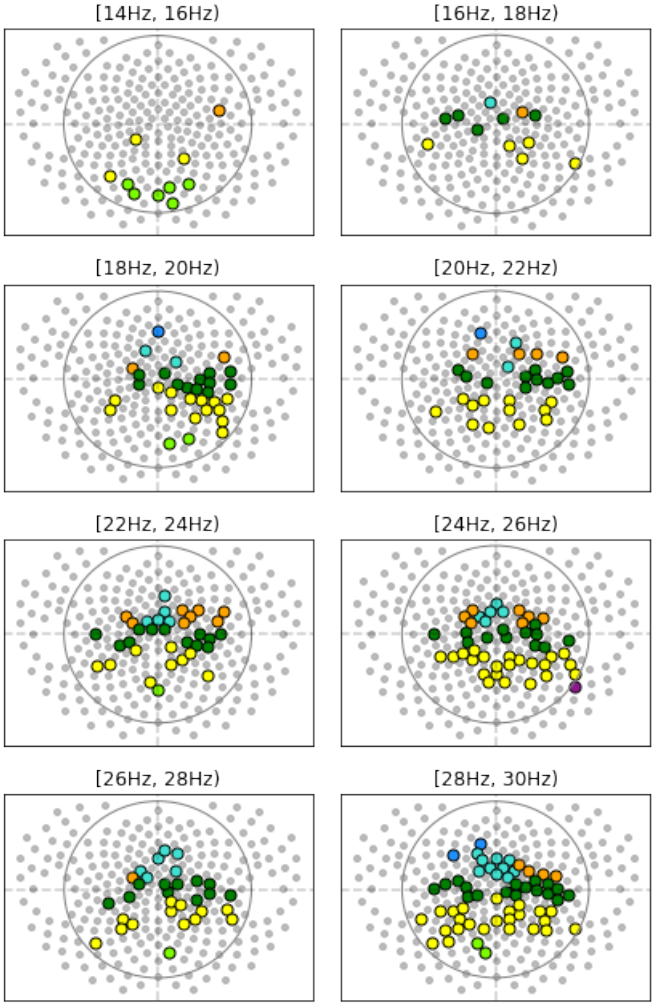

Fig. 5. The 311 features included after anomaly detection and MI feature selection for DBS detection, separated by EEG band. Motor regions are almost exclusively used in this classification, with a tendency towards higher frequency bands.

features selected as a result of anomaly detection and feature selection are illustrated in Figure 7.

To match our DBS detection experiments, we again apply 9-fold cross-validation. However, because each patient only contributes to one class in this dataset, at least two patients must be used in the holdout folds. Thus, for each of the 9 folds, one patient from each class is randomly selected into the holdout fold. Each patient is included in the holdout at least once. This scheme supports a higher number of unique folds with only a fraction of the underlying groups.

The best cross-validation precision scores for each of the 20 models examined are given in Table IV. The holdout results for these models, along with the total count of extracted features, are given in Table V. In contrast to the DBS detection models, we find that random forest based models achieve the best precision, regardless of extraction strategy. Furthermore, the random forest model maintains its performance from the cross-validation set to the holdout, while other low variance

TABLE IV
STIMULATION REGION CLASSIFICATION BEST CV PRECISION SCORES

	CSP	ICA	FC	PCA
GB	0.52	0.60	0.60	0.65
KN	0.52	0.58	0.55	0.52
LR	0.53	0.53	0.52	0.53
RF	**0.59**	**0.63**	**0.61**	**0.65**
SVM	0.57	0.51	0.53	0.52

TABLE V
STIMULATION REGION CLASSIFICATION MODEL PERFORMANCE ON HOLDOUT PATIENTS

	N Extracted	**Accuracy**	**F1**	**Precision**	**Recall**
CSP - SVM	48	**0.66**	0.64	0.68	0.61
PCA - RF	36	0.60	0.58	0.62	0.55
PCA - LR	30	0.54	**0.65**	0.53	**0.85**
ICA - KN	26	0.59	**0.65**	0.58	0.74
PCA - GB	44	0.65	0.62	**0.68**	0.58

models managed to surpass it in holdout performance. The inconsistency between cross-validation scores and holdout scores in this classification tasks suggests a need for better regularization and additional data. This is further explored by producing a learning curve for PCA-RF model, shown in Figure 6. The learning curve results show a clear upward trend in the validation scores, confirming the need for more data in order to avoid spurious correlations.

VI. DISCUSSION & CONCLUSION

We approach the problem of DBS classification using an array of common feature extraction techniques and machine learning models. Results clearly demonstrate successful detection of DBS, as well as classification of DBS region. We find that an SVM applied to features extracted using PCA to be the most precise when detecting DBS across patients. A decision tree-based gradient boosting ensemble, paired with PCA, achieves the highest precision for identifying DBS region. Overall, the majority of models beat the baseline precision, lending support for future effort in this approach to improving DBS efficacy.

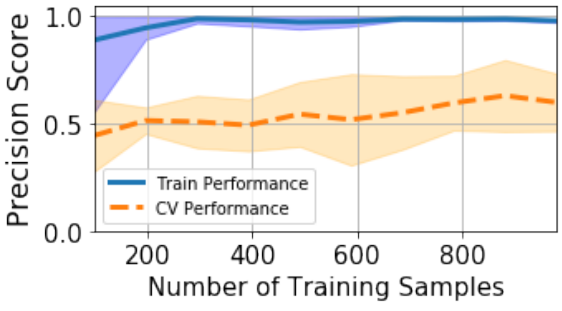

Fig. 6. Learning curve with 9-fold grouped cross-validation for DBS-ON stimulation region classification using PCA-RF model. The model validation scores trend up, suggesting the utility of additional data. However, high variance across folds show the difficulty in generalizing across patients.

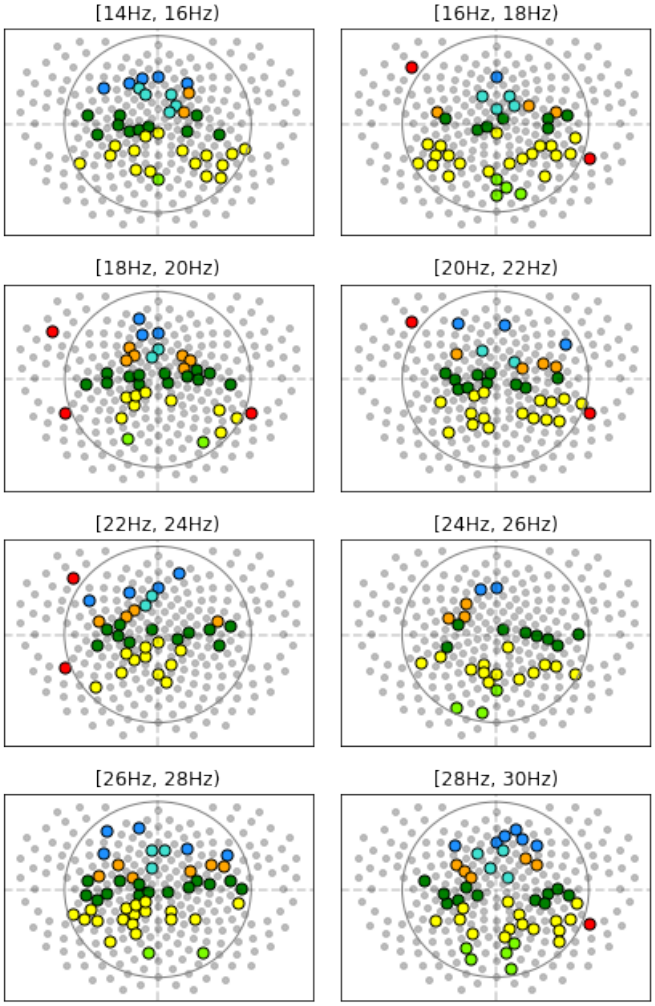

Fig. 7. The 257 features included after anomaly detection and MI feature selection for region classification, separated by EEG band. Motor regions tend to be the most prominently selected feature, aligning with medical understanding of DBS treatment. Temporal regions are rarely selected, while O-T-P is never utilized by the model.

Several areas of our work could be expanded or considered more closely in future work. First, a broader range of feature extraction techniques should be considered, especially those that account for the spatial context of the sensors. This includes how regions may couple in the time and frequency domain, as shown to be relevant in prior work. Additionally, our anomaly treatment strategy may benefit from domain knowledge. For instance, sensor correlation checks may be more sensibly performed with neighbors from within the same brain region only. Other areas of improvement include stronger regularization for both complex models and supervised feature extraction [41].

Finally, we expect our dataset to grow as more patients' DBS implants are tuned with the dense array in place. As evidenced by our learning curve experiments, we expect generalization to improve, possibly leading to novel discoveries in DBS treatment strategies.

ACKNOWLEDGMENT

The authors would like to thank Dr. Kenichiro Ono, Miriam Hirsch, and Rachel Van Aken for their help in recording the dense array EEG data.

REFERENCES

[1] F. M. Weaver, K. A. Follett, M. Stern, P. Luo, C. L. Harris, K. Hur, W. J. Marks, J. Rothlind, O. Sagher, C. Moy, R. Pahwa, K. Burchiel, P. Hogarth, E. C. Lai, J. E. Duda, K. Holloway, A. Samii, S. Horn, J. M. Bronstein, G. Stoner, P. A. Starr, R. Simpson, G. Baltuch, A. De Salles, G. D. Huang, and D. J. Reda, "Randomized trial of deep brain stimulation for Parkinson disease," *Neurology*, vol. 79, no. 1, pp. 55–65, Jul. 2012.

[2] K. A. Follett, F. M. Weaver, M. Stern, K. Hur, C. L. Harris, P. Luo, W. J. Marks, J. Rothlind, O. Sagher, C. Moy, R. Pahwa, K. Burchiel, P. Hogarth, E. C. Lai, J. E. Duda, K. Holloway, A. Samii, S. Horn, J. M. Bronstein, G. Stoner, P. A. Starr, R. Simpson, G. Baltuch, A. De Salles, G. D. Huang, and D. J. Reda, "Pallidal versus Subthalamic Deep-Brain Stimulation for Parkinson's Disease," *New England Journal of Medicine*, vol. 362, no. 22, pp. 2077–2091, Jun. 2010.

[3] F. M. Weaver, K. Follett, M. Stern, K. Hur, C. Harris, W. J. Marks, J. Rothlind, O. Sagher, D. Reda, C. S. Moy, *et al.*, "Bilateral deep brain stimulation vs best medical therapy for patients with advanced parkinson disease: A randomized controlled trial," *Jama*, vol. 301, no. 1, pp. 63–73, 2009.

[4] T. Wichmann and M. R. DeLong, "Deep Brain Stimulation for Neurologic and Neuropsychiatric Disorders," en, *Neuron*, vol. 52, no. 1, pp. 197–204, Oct. 2006.

[5] P. Limousin, P. Pollak, A. Benazzouz, D. Hoffmann, J. F. Le Bas, E. Broussolle, J. E. Perret, and A. L. Benabid, "Effect of parkinsonian signs and symptoms of bilateral subthalamic nucleus stimulation.," English, *Lancet (London, England)*, vol. 345, no. 8942, pp. 91–95, 1995.

[6] D.-B. S. for Parkinson's Disease Study Group, "Deep-brain stimulation of the subthalamic nucleus or the pars interna of the globus pallidus in parkinson's disease," *New England Journal of Medicine*, vol. 345, no. 13, pp. 956–963, 2001.

[7] J. F. Baizabal-Carvallo, M. N. Kagnoff, J. Jimenez-Shahed, R. Fekete, and J. Jankovic, "The safety and efficacy of thalamic deep brain stimulation in essential tremor: 10 years and beyond," en, *Journal of Neurology, Neurosurgery & Psychiatry*, vol. 85, no. 5, pp. 567–572, May 2014.

[8] P. R. Schuurman, D. A. Bosch, P. M. Bossuyt, G. J. Bonsel, E. J. van Someren, R. M. de Bie, M. P. Merkus, and J. D. Speelman, "A Comparison of Continuous Thalamic Stimulation and Thalamotomy for Suppression of Severe Tremor," en, *N Engl J Med*, vol. 342, no. 7, pp. 461–468, Feb. 2000.

[9] W. Lake, P. Hedera, and P. Konrad, "Deep Brain Stimulation for Treatment of Tremor," en, *Neurosurgery Clinics of North America*, vol. 30, no. 2, pp. 147–159, Apr. 2019.

[10] A. Devergnas and T. Wichmann, "Cortical Potentials Evoked by Deep Brain Stimulation in the Subthalamic Area," English, *Front. Syst. Neurosci.*, vol. 5, 2011.

[11] L. Cif, X. Vasques, V. Gonzalez, P. Ravel, B. Biolsi, G. Collod-Beroud, S. Tuffery-Giraud, H. Elfertit, M. Claustres, and P. Coubes, "Long-term follow-up of DYT1 dystonia patients treated by deep brain stimulation: An open-label study: Clinical Course of DYT1 Dystonia with DBS," en, *Mov. Disord.*, vol. 25, no. 3, pp. 289–299, Feb. 2010.

[12] E. F. Chang, L. E. Schrock, P. A. Starr, and J. L. Ostrem, "Long-Term Benefit Sustained after Bilateral Pallidal Deep Brain Stimulation in Patients with Refractory Tardive Dystonia," *SFN*, vol. 88, no. 5, pp. 304–310, 2010.

[13] N. Swann, H. Poizner, M. Houser, S. Gould, I. Greenhouse, W. Cai, J. Strunk, J. George, and A. R. Aron, "Deep Brain Stimulation of the Subthalamic Nucleus Alters the Cortical Profile of Response Inhibition in the Beta Frequency Band: A Scalp EEG Study in Parkinson's Disease," en, *Journal of Neuroscience*, vol. 31, no. 15, pp. 5721–5729, Apr. 2011.

[14] N. C. Swann, C. de Hemptinne, A. R. Aron, J. L. Ostrem, R. T. Knight, and P. A. Starr, "Elevated Synchrony in Parkinson's Disease Detected with Electroencephalography," *Ann Neurol*, vol. 78, no. 5, pp. 742–750, Nov. 2015.

[15] D. D. Wang, C. de Hemptinne, S. Miocinovic, J. L. Ostrem, N. B. Galifianakis, M. San Luciano, and P. A. Starr, "Pallidal Deep-Brain Stimulation Disrupts Pallidal Beta Oscillations and Coherence with Primary Motor Cortex in Parkinson's Disease," en, *J. Neurosci.*, vol. 38, no. 19, pp. 4556–4568, May 2018.

[16] C. de Hemptinne, N. Swann, J. L. Ostrem, E. S. Ryapolova-Webb, M. S. Luciano, N. Galifianakis, and P. A. Starr, "Therapeutic deep brain stimulation reduces cortical phase-amplitude coupling in Parkinson's disease," *Nat Neurosci*, vol. 18, no. 5, pp. 779–786, May 2015.

[17] J. M. Bronstein, M. Tagliati, R. L. Alterman, A. M. Lozano, J. Volkmann, A. Stefani, F. B. Horak, M. S. Okun, K. D. Foote, P. Krack, R. Pahwa, J. M. Henderson, M. I. Hariz, R. A. Bakay, A. Rezai, W. J. Marks, E. Moro, J. L. Vitek, F. M. Weaver, R. E. Gross, and M. R. DeLong, "Deep Brain Stimulation for Parkinson Disease: An Expert Consensus and Review of Key Issues," en, *Arch Neurol*, vol. 68, no. 2, Feb. 2011.

[18] T. Koeglsperger, C. Palleis, F. Hell, J. H. Mehrkens, and K. Bötzel, "Deep Brain Stimulation Programming for Movement Disorders: Current Concepts and Evidence-Based Strategies," English, *Front. Neurol.*, vol. 10, 2019.

[19] J. Volkmann, J. Herzog, F. Kopper, and G. Deuschl, "Introduction to the programming of deep brain stimulators," en, *Movement Disorders*, vol. 17, no. S3, S181–S187, 2002.

[20] R. A. E. Bakay, "Thalamic Deep Brain Stimulation for Essential Tremor: Relation of Lead Location to Outcome," en, *Neurosurgery*, vol. 55, no. 1, pp. 266–267, Jul. 2004.

[21] J. K. Wong, J. H. Cauraugh, K. W. D. Ho, M. Broderick, A. Ramirez-Zamora, L. Almeida, A. Wagle Shukla, C. A. Wilson, R. M. de Bie, F. M. Weaver, N. Kang, and M. S. Okun, "STN vs. GPi deep brain stimulation for tremor suppression in Parkinson disease: A systematic review and meta-analysis," en, *Parkinsonism & Related Disorders*, vol. 58, pp. 56–62, Jan. 2019.

[22] A. M. Kuncel and W. M. Grill, "Selection of stimulus parameters for deep brain stimulation," *Clinical Neurophysiology*, vol. 115, no. 11, pp. 2431–2441, Nov. 2004.

[23] A. Eusebio, A. Pogosyan, S. Wang, B. Averbeck, L. D. Gaynor, S. Cantiniaux, T. Witjas, P. Limousin, J.-P. Azulay, and P. Brown, "Resonance in subthalamo-cortical circuits in Parkinson's disease," en, *Brain*, vol. 132, no. 8, pp. 2139–2150, Aug. 2009.

[24] C. D. MacKinnon, R. M. Webb, P. Silberstein, S. Tisch, P. Asselman, P. Limousin, and J. C. Rothwell, "Stimulation through electrodes implanted near the subthalamic nucleus activates projections to motor areas of cerebral cortex in patients with Parkinson's disease," en, *European Journal of Neuroscience*, vol. 21, no. 5, pp. 1394–1402, 2005.

[25] Z. Ni, S. J. Kim, N. Phielipp, S. Ghosh, K. Udupa, C. A. Gunraj, U. Saha, M. Hodaie, S. K. Kalia, A. M. Lozano, D. J. Lee, E. Moro, A. Fasano, M. Hallett, A. E. Lang, and R. Chen, "Pallidal deep brain stimulation modulates cortical excitability and plasticity," en, *Annals of Neurology*, vol. 83, no. 2, pp. 352–362, 2018.

[26] S. Tisch, J. C. Rothwell, L. Zrinzo, K. P. Bhatia, M. Hariz, and P. Limousin, "Cortical evoked potentials from pallidal

stimulation in patients with primary generalized dystonia," en, *Movement Disorders*, vol. 23, no. 2, pp. 265–273, 2008.

[27] A. W. Laxton, D. F. Tang-Wai, M. P. McAndrews, D. Zumsteg, R. Wennberg, R. Keren, J. Wherrett, G. Naglie, C. Hamani, G. S. Smith, and A. M. Lozano, "A phase I trial of deep brain stimulation of memory circuits in Alzheimer's disease," en, *Ann Neurol.*, vol. 68, no. 4, pp. 521–534, Oct. 2010.

[28] C. Hamani, M. P. McAndrews, M. Cohn, M. Oh, D. Zumsteg, C. M. Shapiro, R. A. Wennberg, and A. M. Lozano, "Memory enhancement induced by hypothalamic/fornix deep brain stimulation," en, *Ann Neurol.*, vol. 63, no. 1, pp. 119–123, Jan. 2008.

[29] J. M. Broadway, P. E. Holtzheimer, M. R. Hilimire, N. A. Parks, J. E. DeVylder, H. S. Mayberg, and P. M. Corballis, "Frontal Theta Cordance Predicts 6-Month Antidepressant Response to Subcallosal Cingulate Deep Brain Stimulation for Treatment-Resistant Depression: A Pilot Study," en, *Neuropsychopharmacology*, vol. 37, no. 7, pp. 1764–1772, Jun. 2012.

[30] G. Pfurtscheller and C. Neuper, "Motor imagery and direct brain-computer communication," *Proceedings of the IEEE*, vol. 89, no. 7, pp. 1123–1134, Jul. 2001.

[31] G. Townsend, B. Graimann, and G. Pfurtscheller, "Continuous EEG Classification During Motor Imagery—Simulation of an Asynchronous BCI," en, *IEEE Trans. Neural Syst. Rehabil. Eng.*, vol. 12, no. 2, pp. 258–265, Jun. 2004.

[32] Yijun Wang, Shangkai Gao, and Xiaornog Gao, "Common Spatial Pattern Method for Channel Selelction in Motor Imagery Based Brain-computer Interface," in *2005 IEEE Engineering in Medicine and Biology 27th Annual Conference*, Shanghai, China: IEEE, 2005, pp. 5392–5395.

[33] T. Kalayci and O. Ozdamar, "Wavelet preprocessing for automated neural network detection of EEG spikes," *IEEE engineering in medicine and biology magazine*, vol. 14, no. 2, pp. 160–166, 1995.

[34] A. T. Tzallas, M. G. Tsipouras, and D. I. Fotiadis, "Epileptic Seizure Detection in Electroencephalograms using Time-Frequency Analysis," en, p. 9,

[35] T. T. Erguzel, S. Ozekes, S. Gultekin, N. Tarhan, G. Hizli Sayar, and A. Bayram, "Neural Network Based Response Prediction of rTMS in Major Depressive Disorder Using QEEG Cordance," *Psychiatry Investig*, vol. 12, no. 1, pp. 61–65, Jan. 2015.

[36] J. Rumiński, "Reliability of Pulse Measurements in Videoplethysmography," en, *Metrology and Measurement Systems*, vol. 23, no. 3, pp. 359–371, Sep. 2016.

[37] A. Secerbegovic, J. Bergsland, P. Halvorsen, N. Suljanovic, A. Mujcic, and I. Balasingham, "Blood pressure estimation using video plethysmography," en, in *2016 IEEE 13th International Symposium on Biomedical Imaging (ISBI)*, Prague, Czech Republic: IEEE, Apr. 2016, pp. 461–464.

[38] B. Iglewicz and D. C. Hoaglin, *How to detect and handle outliers*, en, ser. ASQC basic references in quality control v. 16. Milwaukee, Wis: ASQC Quality Press, 1993.

[39] F. Pedregosa, G. Varoquaux, A. Gramfort, V. Michel, B. Thirion, O. Grisel, M. Blondel, P. Prettenhofer, R. Weiss, V. Dubourg, J. Vanderplas, A. Passos, D. Cournapeau, M. Brucher, M. Perrot, and E. Duchesnay, "Scikit-learn: Machine learning in Python," *Journal of Machine Learning Research*, vol. 12, pp. 2825–2830, 2011.

[40] H. Ramoser, J. Muller-Gerking, and G. Pfurtscheller, "Optimal spatial filtering of single trial EEG during imagined hand movement," en, *IEEE Trans. Rehab. Eng.*, vol. 8, no. 4, pp. 441–446, Dec. 2000.

[41] F. Lotte and C. Guan, "Regularizing common spatial patterns to improve bci designs: Unified theory and new algorithms," *IEEE Transactions on biomedical Engineering*, vol. 58, no. 2, pp. 355–362, 2010.